processes

MDPI

Article

Numerical Analysis and Optimization of Load Uniformity in a Coiled Tubing Injector Head Clamping System for Deep Well Operations

Gao Yang [1], Hao Jiang [2,*], Fei Liu [1], Zhiliang Gai [1], Wencai Yuan [1], Jiawei Liu [1], Huaizhou Wei [2] and Can Cai [2]

[1] Jianghan Machinery Research Institute Co., Ltd. of China National Petroleum Corporation (CNPC), Wuhan 430223, China
[2] High-Pressure Jet Theory and Application Technology Laboratory, School of Mechanical Engineering, Southwest Petroleum University, Chengdu 610500, China
* Correspondence: jhhh666888@163.com; Tel.: +86-17815363982

Abstract

As downhole operation depth increases, the structural optimization of the coiled tubing injector head clamping system becomes increasingly critical for deep well operations. This study addresses key issues, including insufficient clamping normal force, severe stress concentration and tubing damage, through mechanical analysis, numerical simulation and structural optimization. A numerical model of the clamping system was established to investigate gripper block load distribution, the effects of key structural parameters, and stress–strain characteristics of coiled tubing with residual bending. The results show that loads on individual gripper blocks are unevenly distributed, with the standard deviation of normal force increasing linearly with clamping force. Optimal load uniformity is achieved when the gripper block spacing is 5 mm, and the clamping beam spacing equals the ratio of push plate length to the number of clamping beams. These findings provide theoretical guidance for developing high-performance injector heads.

Keywords: coiled tubing; injector head; clamping system; load distribution; gripper block

1. Introduction

With sustained economic development and increasing energy demand, oil and gas extraction has entered the stage of deep and ultra- deep wells, which makes the exploration and extraction of deep geological resources face more and more problems [1–3]. Moreover, as well depth increases, the required length of coiled tubing also increases. Ultra-deep wells are also characterized by more complex formation structures and higher downhole pressures, which increase the axial load, formation pressure, and upward force acting on the coiled tubing [4–6]. Consequently, higher performance requirements are imposed on the injector head and gripper blocks of coiled tubing units. As critical components in direct contact with the coiled tubing, gripper blocks must provide sufficient clamping force to enable tubing running and retrieval while minimizing clamping-induced damage, thereby ensuring the service life of coiled tubing in complex deep geological environments [7,8]. Therefore, improving the lifting capacity of the injector head has become an important research objective in drilling engineering.

Coiled tubing technology primarily consists of three components: coiled tubing unit, downhole tools, and operational procedures (Figure 1). Specifically, the coiled tubing unit mainly includes a reel, a gooseneck, an injector head, and coiled tubing [9]. The

Check for updates

Academic Editor: Dongmei Wang

Received: 28 October 2026
Revised: 16 November 2026
Accepted: 26 November 2026
Published: 27 November 2026

Copyright: © 2026 by the authors. Licensee MDPI, Basel, Switzerland. This article is an open access article distributed under the terms and conditions of the Creative Commons Attribution (CC BY) license.

maximum working load of a coiled tubing injector head is primarily determined by the hydraulic driving force in the chain system and the clamping force provided by the gripper blocks [10]. Sufficient clamping force is essential to ensure stable running and retrieval of the coiled tubing.

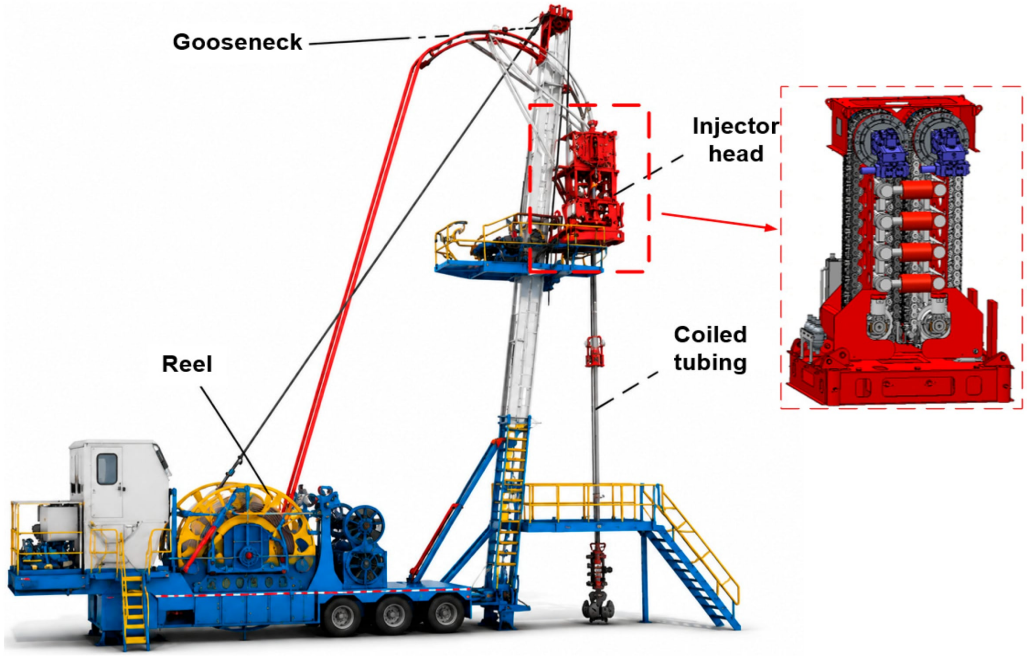


Figure 1. Coiled tubing unit and injector head.

In ultra-deep well operations, the injector head of coiled tubing equipment is constrained by size limitations, making it difficult to further increase the driving force provided by the hydraulic system and resulting in insufficient clamping force [11]. Meanwhile, to prevent severe clamping-induced damage to the coiled tubing, the clamping force cannot be increased without limit. Consequently, it is difficult to overcome the current operational capacity bottleneck solely by upgrading the hydraulic system. Therefore, research on enhancing the maximum operating capacity of coiled tubing units has mainly focused on improving the gripping capacity of gripper blocks while reducing clamping-induced damage to the coiled tubing [12]. Overall, existing studies on gripper blocks have mainly focused on the effects of geometric parameters on the normal contact pressure and friction coefficient at the tubing surface, the force analysis of gripper blocks during operation, the tubing-block contact behavior, and the stress distribution in coiled tubing [13].

The V-shaped gripper block was improved by dividing it into a gripper block body and an arched gripping plate, with an elastic cushion inserted between them [14,15]. By adjusting the elastic cushion, the gripper block can more readily accommodate coiled tubing of different sizes. Moreover, the effects of trapezoidal-groove and elliptical-groove gripper block structures on the clamping stress and contact area of coiled tubing were investigated, and it was found that the maximum von Mises stress of the trapezoidal-groove gripper block gradually increased with increasing groove depth but decreased with increasing tooth profile angle [16]. In studies on clamping mechanisms and mechanical modeling, A theoretical model for the friction resistance coefficient was established, and it was proposed that the friction coefficient between the coiled tubing and the gripper blocks decreases with increasing normal force. In addition, the overall clamping performance of semicircular, V-shaped, and four-lobe gripper blocks was compared [17]. Moreover, the effects of factors such as coiled tubing wall thickness on fatigue life during tripping

operations were investigated, and a fatigue life prediction model for coiled tubing between the reel and the injector head was established based on the Manson–Coffin equation and linear damage accumulation theory [4]. The interaction between the gripper blocks and the coiled tubing was optimized by considering the combined effects of axial tensile force, internal fluid pressure, and clamping force, and it was found that gripper blocks with a half-spacing of 8 mm could minimize damage to the coiled tubing [18]. Moreover, based on fundamental dynamic theory, a multibody dynamic model of the injector head clamping system was established to investigate the effects of clamping force and tensile force on the impact collision between the gripper blocks and the slide plate [19].

To date, studies on the clamping performance of injector heads have largely focused on a single set of gripper blocks and have generally assumed that all gripper blocks across the clamping region are subjected to uniform loading [5]. However, limited attention has been paid to the actual load distribution among individual gripper blocks within this region [8]. Therefore, to mitigate the risk of localized indentation and stress-induced damage to the coiled tubing caused by excessive loading on individual gripper blocks within the clamping region, this work investigates the uniform load distribution design of the entire injector head clamping system. Improving load uniformity can effectively reduce the local peak stress level of the tubing, which serves as a favorable prerequisite for alleviating fatigue damage accumulation and extending tubing service life. This study developed a numerical model of the injector head clamping system to analyze the load distribution among individual gripper blocks across the entire clamping region. A single factor analysis was then performed to investigate the effects of the gripper block arrangement, clamping-beam spacing, and clamping force on load-distribution uniformity.

2. Structural Force Analysis and Model Development of the Clamping System

2.1. Structure and Working Principle of the Coiled Tubing Injector Head

As a well-recognized basic law in coiled tubing engineering, the force state of the coiled tubing varies dynamically with well depth and tubing string length [9,10]. This study takes this law as the analytical basis and further develops the refined calculation of axial load and the investigation of clamping system load distribution. The structure of the internal clamping system of the injector head is shown in Figure 2. The clamping system mainly consists of hydraulic cylinders, clamping beams, push plates, rollers, carriers, and gripper blocks. During clamping of the coiled tubing, the hydraulic cylinders drive the clamping beams toward the coiled tubing. The clamping force is then transmitted sequentially through the push plates, rollers, carriers, and gripper blocks. Finally, the static friction generated by the gripper blocks balances the axial load acting on the coiled tubing, thereby securely gripping the coiled tubing.

The force interaction between the gripper blocks and the coiled tubing during injector head operation is shown in Figure 3. The gripper blocks press against the coiled tubing under the clamping force F_0 applied by the hydraulic clamping system. The resulting static friction between the gripper blocks and the coiled tubing counteracts the axial force F_a, thereby maintaining relative static contact between them [9]. Meanwhile, the sprocket assembly drives the gripper blocks to move cyclically, enabling the running and retrieval of the coiled tubing.

As the depth of the coiled tubing in the well changes, its axial force varies accordingly, and the clamping force provided by the injector head should be adjusted correspondingly. Furthermore, as the downhole tubing length increases, the required maximum working load of the injector head also increases to ensure the normal operation of the coiled tubing.

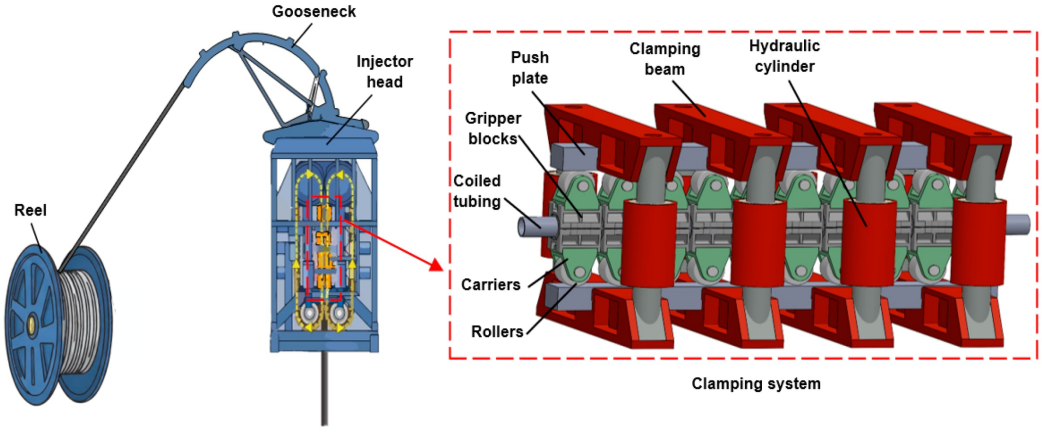


Figure 2. Clamping system of the injector head.

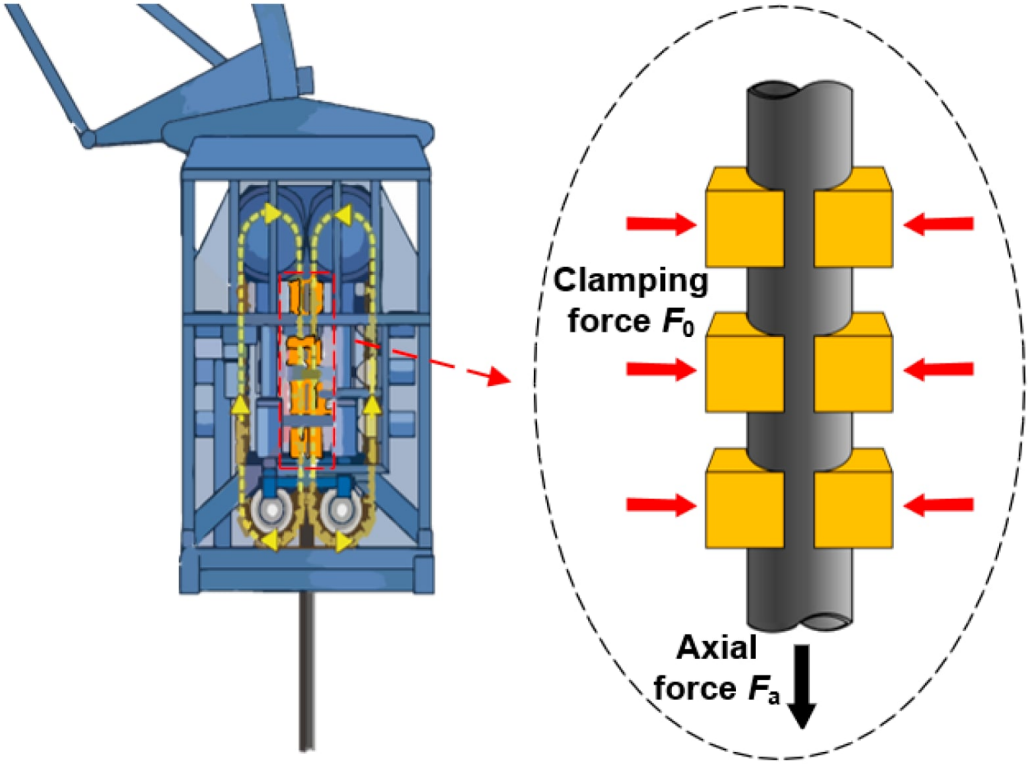


Figure 3. The force analysis of the gripper block and coiled tubing.

2.2. Axial Load

During coiled tubing running and retrieval, the axial force acting on the coiled tubing mainly includes its self-weight in the wellbore, the upward force exerted by the wellbore pressure, the friction force between the coiled tubing and components such as the wellbore wall and blowout preventer, and the dynamic load of the coiled tubing. The axial force model during coiled tubing running and retrieval is shown in Figure 4.

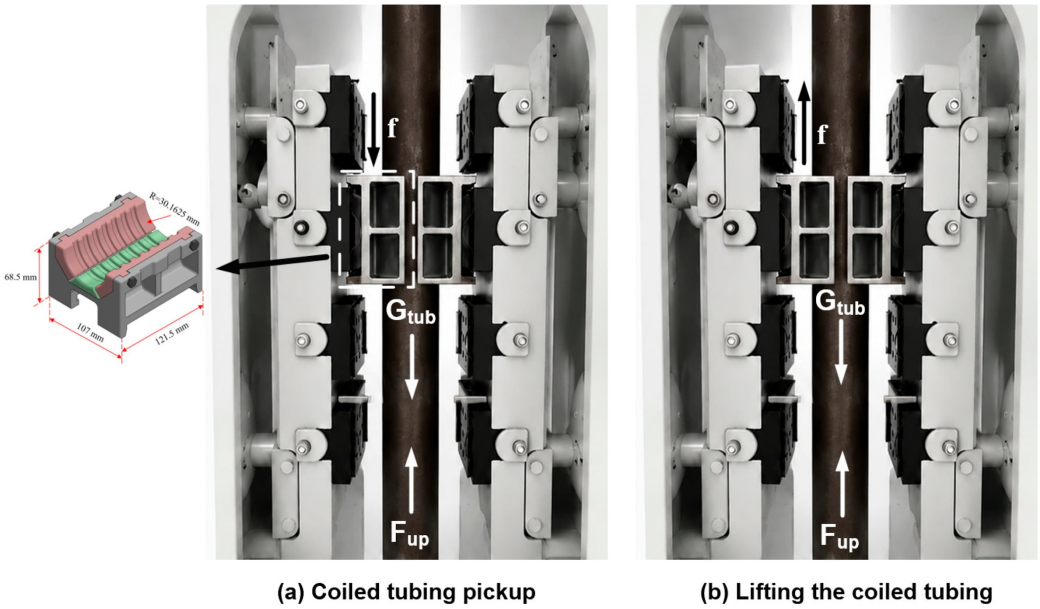


Figure 4. Axial force model of coiled tubing.

As shown in Figure 4, the forces acting on the downhole coiled tubing mainly include the following components:

Tubing string weight G_{tub}: the self-gravity of the coiled tubing string, acting vertically downward along the wellbore; Wellbore upward force F_{up}: the buoyancy force exerted by the drilling fluid on the tubing string, acting vertically upward along the wellbore; Wellbore friction force f: the axial friction resistance between the tubing and the wellbore wall, whose direction is opposite to the movement direction of the coiled tubing; Axial load F_a: the axial force acting on the upper end of the tubing string.

During coiled tubing operations, a check valve is installed at the lower end of the tubing to prevent upward transmission of wellbore pressure. Therefore, the upward force can be assumed to act continuously on the lower end of the tubing. In addition, the stable hydraulic system of the injector head allows the coiled tubing to be run and retrieved at an approximately constant speed; thus, the dynamic load of the tubing can be neglected. Based on these assumptions, the axial force of the coiled tubing can be expressed with the following Equation (1) [10]:

$$F_{\mathrm{a}} = \frac{\pi}{4} D^2 (P_0 + \rho_m g h) - \frac{\pi}{4} (D^2 - d^2) \rho_s g h \pm f \tag{1}$$

where F_a is the axial force of the coiled tubing; P_0 is the wellhead pressure; ρ_m is the drilling fluid density; ρ_s is the density of the coiled tubing material; h is the running depth of the coiled tubing; D is the outer diameter of the coiled tubing; d is the inner diameter of the coiled tubing; and f is the axial friction force acting on the coiled tubing.

Physically, Equation (1) is composed of three independent force components, which are fully consistent with the force descriptions presented earlier and the labels in Figure 4:

The tubing string weight term, corresponding to G_{tub} in Figure 4: it originates from the self-gravity of the coiled tubing string, and its magnitude is determined by the tubing material density, cross-sectional area and well depth, acting vertically downward along the wellbore;

The wellbore upward force term, corresponding to F_{up} in Figure 4: it is generated by the combined action of wellhead pressure and drilling fluid buoyancy, acting vertically upward to offset part of the tubing weight;

The friction force term $\pm f$, corresponding to the wellbore friction force described above: it represents the axial friction resistance between the tubing and the wellbore wall, with its sign determined by the movement direction of the coiled tubing.

The axial force of the coiled tubing during pull-out can be expressed with the following Equation (2):

$$F_{\text{up}} = \frac{\pi}{4} D^2 [P_0 - (1 - \frac{d^2}{D^2}) \rho_s g h] \quad (2)$$

The axial force of the coiled tubing during run-in can be expressed with the following Equation (3):

$$F_{\text{d}} = \frac{\pi}{4} D^2 [P_0 + 2\rho_m g h - (1 - \frac{d^2}{D^2}) \rho_s g h] \quad (3)$$

The sign convention for the friction force term f in the axial load formulas is explicitly defined as follows: the wellbore friction force always acts in the direction opposite to the movement of the coiled tubing.

For the tripping-out (pull-out) condition corresponding to Equation (2), the coiled tubing moves upward along the wellbore, and the friction force acts downward, consistent with the direction of tubing string weight. Thus, the friction term takes a positive sign $(+f)$ and is superimposed with the self-weight to increase the total axial load.

For the tripping-in (run-in) condition corresponding to Equation (3), the coiled tubing moves downward along the wellbore, and the friction force acts upward, opposite to the direction of tubing string weight. Thus, the friction term takes a negative sign $(-f)$ and partially offsets the self-weight to reduce the total axial load.

2.3. Simulation Methods and Verification

Figure 5 illustrates the force interaction between the injector head clamping system and the coiled tubing. Specifically, the push plates are subjected to the thrust exerted by the clamping beams, which is transmitted through the gripper blocks and converted into the normal clamping force acting on the coiled tubing. Therefore, analyzing the uniformity of load distribution in the clamping system is essentially equivalent to evaluating the differences in the clamping normal force between each gripper block and the coiled tubing.

2.3.1. Numerical Modeling

Taking a specific injector head as an example, the entire clamping region contains 10 pairs of effective gripper blocks, and four sets of clamping beams are arranged on the push plates. The coiled tubing has an outer diameter of 2–3/8 in. To reduce the computational cost, the hydraulic cylinders are simplified, and equivalent concentrated thrust loads are applied on the end faces of each clamping beam, with the load direction pointing toward the central axis of the coiled tubing. The numerical model of the clamping system is shown in Figure 6. The coiled tubing has a length of 200 mm and a wall thickness of 4.8 mm. The relevant dimensional parameters of the semi-circular and V-shaped gripper blocks are consistent with those of the aforementioned combined three-segment gripper blocks. According to the Coiled Tubing Engineering Technical Manual, the coiled tubing is made of CT110 and the gripper blocks are made of 20CrNiMo. The mechanical properties of the two materials are summarized in Table 1.

The established geometric model is imported into Abaqus for meshing, and the resulting finite element model is illustrated in Figure 6. Specifically, the coiled tubing is meshed with hexahedral elements of type C3D8R at a mesh size of 2 mm; the gripper blocks are meshed with tetrahedral elements of type C3D10 at a mesh size of 3 mm.

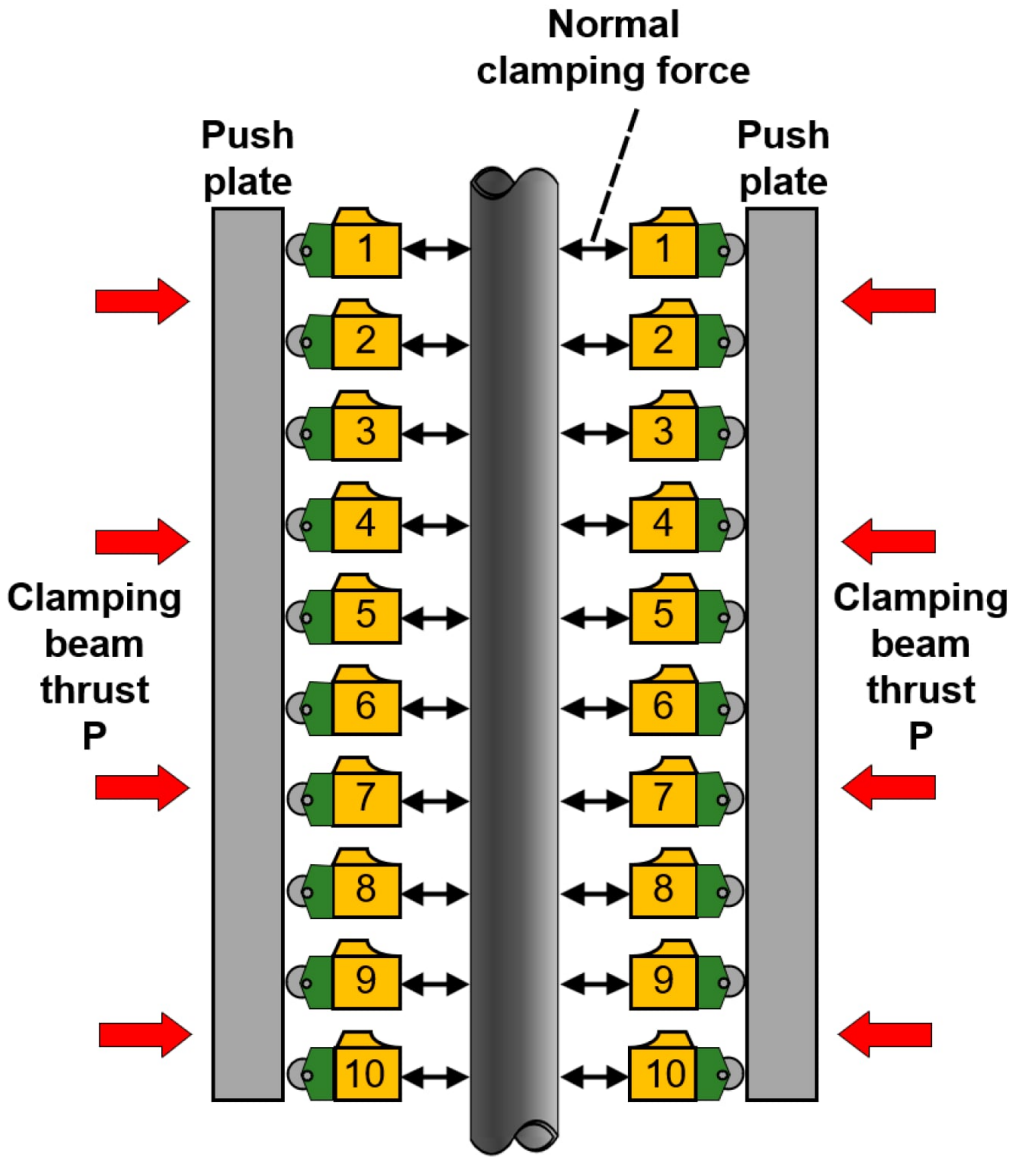


Figure 5. Force analysis diagram of the clamping system.

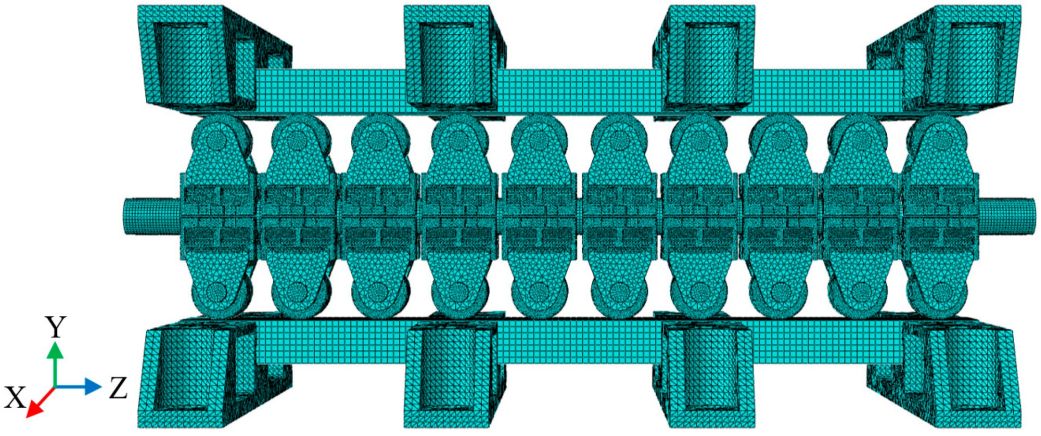


Figure 6. Numerical model of the clamping system.

Table 1. Material and Mechanical Properties of Coiled Tubing and Gripper Blocks.

Parameter	Coiled Tubing	Gripper Block
Material	CT110	20CrNiMo
Elastic modulus/GPa	240	205
Poisson's ratio	0.3	0.3
Yield strength/MPa	787	785
Gripper block spacing: 5 mm	390.71	254.01
Gripper block spacing: 2.5 mm	396.40	256.27

Accordingly, contact interactions were defined between the clamping beam and push plate, push plate and roller, roller and bracket, bracket and gripper block, and gripper block and coiled tubing. Since the core objective of this study is to reveal the distribution pattern and uniformity characteristics of the normal clamping force among individual gripper blocks in the clamping system, with emphasis on the relative load distribution ratio across multiple gripper blocks, the axial load on the coiled tubing is not considered in the current numerical modeling. This simplification is mechanically well-justified for the following reasons: (1) In accordance with Saint-Venant's principle, the axial tensile force acts as a uniformly distributed global tensile stress along the cross-section of the tubing. It only superimposes on the overall stress level of the coiled tubing, without modifying the normal contact pressure distribution at the contact interface between the gripper blocks and the tubing, nor affecting the relative load distribution ratio among individual gripper blocks. (2) This simplification has also been widely adopted in similar studies focusing on the gripping performance and load distribution of gripper blocks [18], to concentrate the analysis on the normal contact transmission mechanism and load distribution behavior. Based on the rated working load of the injector head, a thrust force of 112.5 kN was applied to both ends of each clamping beam along the Y-direction toward the coiled tubing.

The correspondence among the applied beam loads, the nominal clamping force and the forces on individual gripper blocks is explicitly clarified as follows. The 112.5 kN concentrated load applied at each loading position of the clamping beams serves as the input load of the finite element model. Through the force transmission chain consisting of clamping beams, push plates, rollers and carriers, the input load is converted into normal clamping forces acting on all gripper blocks, and this transmission relationship is also consistent with the theoretical calculation formula derived in Section 2.3.2. Under this loading scheme, the average normal clamping force borne by each pair of gripper blocks is approximately 180 kN, which corresponds to the nominal clamping force parameter commonly adopted in engineering design. Affected by the bending deformation of the push plate, the actual load of each gripper block at different positions deviates from the average value, and the detailed distribution law is systematically analyzed in the subsequent sections.

Figure 7 shows the stress distribution contours of the components in the clamping system. The maximum von Mises stresses of the clamping beam, push plate, roller, bracket, gripper block, and coiled tubing are 175.28, 294.20, 528.70, 211.72, 353.18, and 136.99 MPa, respectively. These values are lower than the corresponding yield strengths, indicating that all components satisfy the strength requirements. Furthermore, the stress-field distributions differ markedly among the individual rollers, brackets, and gripper blocks. To facilitate the analysis, the roller-bracket-gripper block assemblies are numbered from 1 to 10 from left to right, as shown in Figure 7. The high-stress regions on the surfaces of rollers 1, 4, 7, and 10 are more concentrated and cover larger areas, whereas those on the remaining rollers are relatively limited. Similarly, the support bracket group and gripper block group exhibit stress distributions consistent with those of the roller group. This difference is mainly attributed to the nonuniform distribution of contact loads between the rollers and the push plate.

Specifically, variations in contact conformity and loading angle between different rollers and the clamped components cause some rollers to carry a larger portion of the transmitted load. Consequently, these rollers exhibit higher local stress levels, whereas rollers sharing less load show relatively lower stress levels. Consequently, the clamping-force transmission between each gripper block and the coiled tubing becomes nonuniform. The gripper blocks located near the clamping beam are subjected to higher local loads and, therefore, exhibit higher stress levels. The individual differences among the rollers, brackets, and gripper-block groups essentially result from the combined effects of component installation position, load-transfer path, and contact state. This finding provides a targeted basis for subsequently optimizing the load-distribution uniformity of the clamping system.

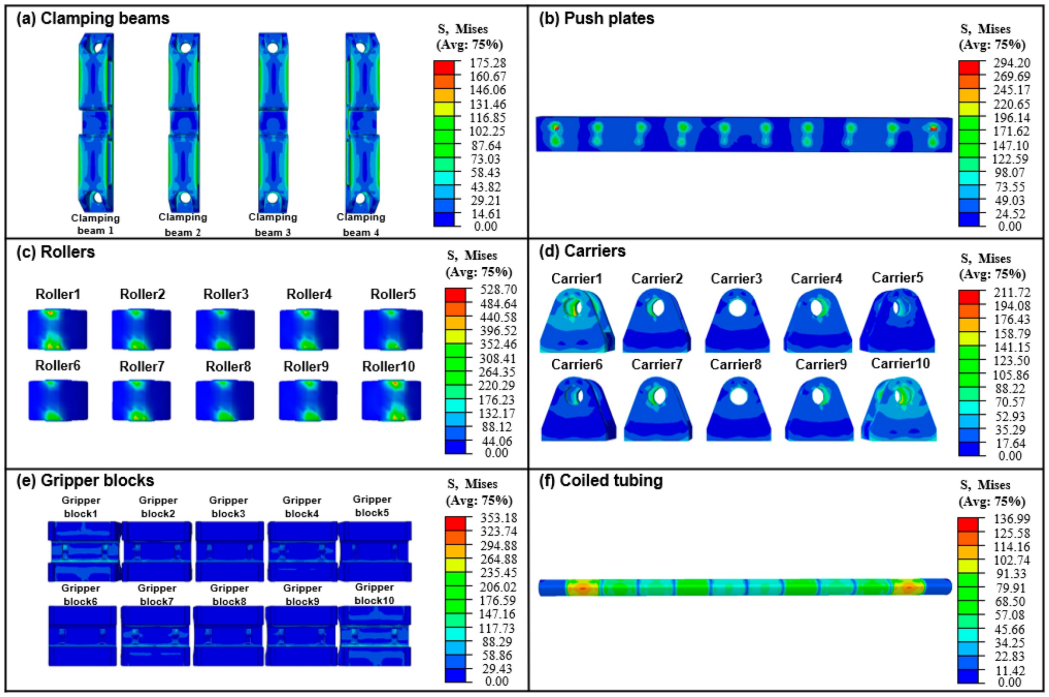


Figure 7. Stress contours of each component in the clamping system.

2.3.2. Model Verification

To verify the accuracy of the theoretical solution, a three-dimensional finite element clamping model was established based on the technical specifications of an injector head developed by Jianghan Machinery Research Institute. In addition, the basic parameters for the gripper blocks clamping the coiled tubing were determined according to the technical standards in the Coiled Tubing Engineering Technology Manual [20,21], as follows:

The vertical well depth was 10,000 m; the coiled tubing size was 2–3/8 in. with an outer diameter of 60.325 mm, an inner diameter of 50.725 mm, and a wall thickness of 4.8 mm; the axial load was 615 kN; the fluid pressure was 120 MPa; the number of effective gripper-block pairs was 10; and the number of clamping cylinders was 8.

Since the clamping force acting on the gripper blocks is provided by the clamping cylinders, friction among the internal mechanisms of the injector head must be considered when calculating the required clamping force to prevent slippage. Therefore, the load on each clamping cylinder can be expressed with the following Equation (4):

$$F_i = \frac{C_d F_{max}}{n_0 \mu} \tag{4}$$

where C_d is the friction amplification coefficient, with C_d = 1.2~1.3; Fmax is the maximum axial load at the injector head; n_0 is the number of gripper blocks; and μ is the friction coefficient between the gripper blocks and the coiled tubing.

Equation (4) presents the calculation formula for the thrust of a single clamping cylinder. To ensure consistent force definitions throughout the manuscript, the quantities of key components and the force-transfer relationship are uniformly specified as follows:

(1) Total number of clamping cylinders: 8, symmetrically arranged on both sides of the clamping system; (2) Total number of effective gripper block pairs: 10, axially distributed along the coiled tubing in the clamping region.

The total thrust output by all clamping cylinders is transmitted to each gripper block pair sequentially through the force transmission chain of clamping beams, push plates, rollers and carriers. Under the reference working condition, the single-cylinder thrust calculated by Equation (4) is 222.28 kN. After force transmission and load distribution, the average normal clamping force borne by each pair of gripper blocks is approximately 180 kN, which is consistent with the nominal clamping force parameter adopted in the parametric analysis sections. The load difference among gripper blocks at different positions, induced by the bending deformation of the push plate during force transmission, constitutes the core focus of the load distribution study in this paper.

Under the assumption of uniform load sharing among all gripper blocks, the average normal clamping force borne by each pair of gripper blocks can be derived from the total thrust of the clamping cylinders, as expressed in Equation (5):

$$F_{pair} = \frac{n_{cyl} \cdot F_{cyl}}{n_0} \tag{5}$$

where n_{cyl} is the total number of clamping cylinders, F_{cyl} is the thrust of a single cylinder calculated by Equation (4), and n_0 is the total number of effective gripper block pairs.

Assuming that each pair of gripper blocks is subjected to the same clamping force, with C_d = 1.3 and μ = 0.45, the load on each clamping cylinder was calculated using the corresponding equation to be 222.28 kN, and the clamping force acting on each pair of gripper blocks was 177.83 kN.

To facilitate the calculation, one pair of gripper blocks was selected for analysis. The clamping force applied to each gripper block was 90 kN, and the axial load on the coiled tubing was 62 kN.

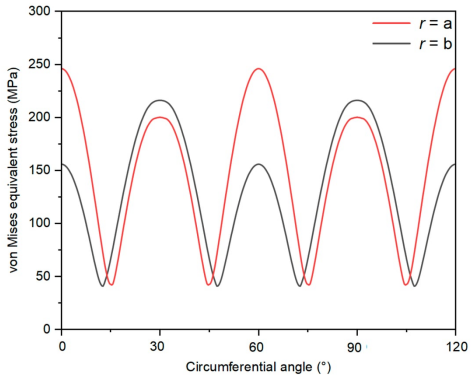
Based on the thick-walled cylinder Lame theory and the elastic solution for partial external pressure, the stress state of the coiled tubing under local clamping load can be theoretically derived. For a tubing with inner radius a and outer radius b subjected to uniformly distributed contact pressure within the contact half-angle β, the radial stress σ_r, hoop stress σ_θ and axial stress σ_z at any position can be obtained. The von Mises equivalent stress is further synthesized by three principal stresses, as expressed in Equation (6):

$$\sigma_{von} = \frac{1}{\sqrt{2}} \sqrt{(\sigma_z - \sigma_\theta)^2 + (\sigma_\theta - \sigma_z)^2 + (\sigma_z - \sigma_r)^2} \tag{6}$$

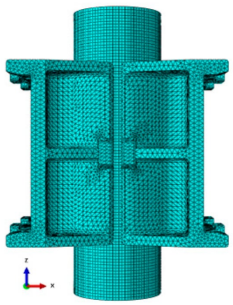
For the clamping condition in this study, the maximum von Mises stress occurs on the inner wall of the tubing $r = a$ at the gap between adjacent gripper blocks, which is dominated by the superposition of hoop tensile stress and axial compressive stress.

By substituting the above parameters into the von Mises equivalent stress expression for the coiled tubing, the circumferential stress distributions on the inner and outer walls of the tubing can be obtained, as shown in Figure 8a. The stress distributions on the inner wall ($r = a$) and outer wall ($r = b$) show opposite peak positions: the maximum von Mises stress of 246.05 MPa occurs on the inner wall ($r = a$) at the gap positions between adjacent gripper blocks (corresponding to 0°, 60° and 120° on the horizontal axis), while the stress peak on

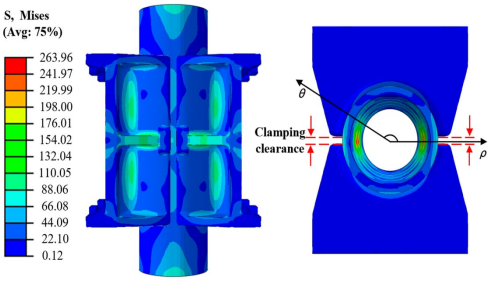
the outer wall ($r = b$) appears at the center of the gripper block contact area (corresponding to 30° and 90° on the horizontal axis).



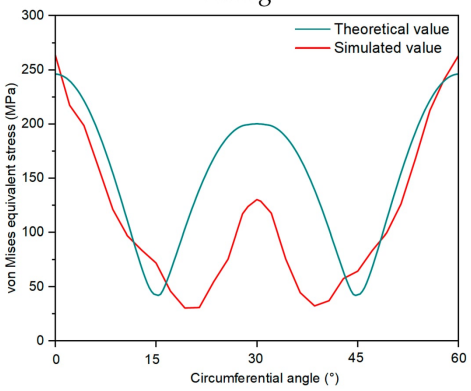
(**a**) Comparison of theoretical and finite element results



(**b**) Model of the gripper block clamping coiled tubing



(**c**) Mises equivalent stress contour plot of the coiled tubing clamped by the gripper block



(**d**) Circumferential von Mises stress of coiled tubing

Figure 8. Finite element analysis and stress distribution of coiled tubing under clamping.

The finite element stress contour obtained from the numerical simulation is shown in Figure 8c. The overall maximum von Mises stress in the coiled tubing occurs on its inner surface at the clamping gaps between adjacent gripper blocks, which is fully consistent with the peak position of the theoretical solution. The maximum stress value is 263.96 MPa, and the relative error compared with the theoretical result is 7.28%, which is within the acceptable engineering error range.

Owing to the central symmetry of the model, the nodal stresses along the circumferential path on the inner surface of the coiled tubing within a single gripper block contact range (0–60°) were extracted. The variation in these stresses with the circumferential angle was then plotted and compared with the theoretical results, as shown in Figure 8d. A comparison between the theoretical von Mises stresses and the finite element results shows that both stress curves exhibit consistent circumferential variation trends. The stress reaches the minimum at the center of the contact area (30°) and peaks at the edges of the contact area (0° and 60°, i.e., the gap between adjacent gripper blocks), presenting a typical W-shaped variation pattern. This distribution law is completely consistent with the full-circumference result shown in Figure 8a.

The total normal contact force between a single pair of gripper blocks and the coiled tubing is obtained by integrating the uniform contact pressure along the circumferential contact arc. The corresponding theoretical calculation formula is expressed as Equation (7):

$$F_n = \int_{-\beta}^{\beta} pbd\theta = 2pb\beta \quad (7)$$

where p is the uniform contact pressure on the tubing surface, b is the outer radius of the coiled tubing, and β is the half contact angle of the gripper block.

Substituting the above clamping parameters, namely $F_0 = 180$ and $\beta = 14.5°$, into the theoretical equation for the normal force gives a normal force of 244.99 kN on the surface of the coiled tubing. In the finite element model, the normal force on the coiled tubing surface was obtained by summing the contact forces over all elements on its outer surface, yielding 231.39 kN. Therefore, the relative error between the theoretical and finite element normal forces is 5.88%, which is within the allowable error range. These results validate the accuracy of the theoretical solution and provide theoretical guidance for the subsequent investigation of the structural performance of the coiled tubing and gripper blocks.

To further verify the reliability of the load transmission and distribution characteristics of the complete clamping system comprising 10 pairs of effective gripper blocks and 4 sets of clamping beams, this study performs system-level benchmark validation using load data from industrial-type tests of an identical coiled tubing injector head provided by Jianghan Machinery Research Institute Co., Ltd. The test specimen is an injector head with the same specifications as the simulation model in this work. Thin-film pressure sensors were employed to collect the normal contact loads of gripper blocks at different positions within the clamping region under the rated clamping force condition. Test results indicate that the ratio of normal load between the end gripper blocks and the middle gripper blocks is approximately 2.1:1 under the rated condition, and the overall axial load distribution exhibits a pattern of "high values at both ends and fluctuations in the middle". The ratio of the maximum to minimum gripper block load obtained from the numerical simulation is about 2.15:1. The overall distribution trend is in excellent agreement with the experimental measurements, with a relative deviation of the load ratio below 2.4%. This benchmark verification confirms that the established full clamping system numerical model can accurately reflect the load transmission law across clamping beams, push plates, rollers and gripper blocks, and the system-level calculation results possess sound engineering reliability.

3. Results and Discussions

3.1. Load Distribution Pattern of Each Gripper Block

Owing to the structural and loading symmetry of the gripper blocks and coiled tubing in the clamping region of the injector head, five gripper-block groups, numbered 1–5, and their corresponding tubing sections in the upper half of the clamping system along the symmetry axis were selected for analysis, as shown in Figure 9.

According to the theoretical analysis of clamping mechanics and the numerical simulation of a single gripper block, the maximum stress and strain in the coiled tubing occur at the clamping gaps between the gripper blocks on both sides. As shown in Figure 9a,b, the von Mises stress and strain of the coiled tubing are nonuniformly distributed along the axial direction. In particular, the stress and strain in the region corresponding to gripper block 1 are much higher than those in the regions corresponding to the other gripper blocks. The axial distributions of stress and strain in the same region of the coiled tubing indicate that, within the central region of the clamping contact surface, the von Mises stress exhibits a peak-shaped distribution along the axial direction, whereas the strain exhibits a

valley-shaped distribution. Both quantities decrease sharply at the edges of the clamping contact surface and in the gaps between adjacent gripper blocks. During running-in and pulling-out operations, the nonuniform loading of the tubing sections corresponding to different gripper blocks may promote fatigue failure of the coiled tubing. Therefore, the load uniformity among the gripper blocks should be improved as much as possible in the design of the clamping system.

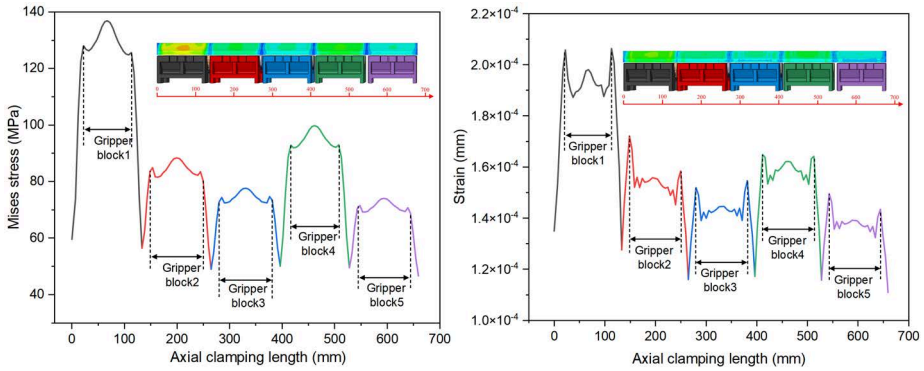


Figure 9. Distribution of axial stress and strain of coiled tubing at the clamping clearance.

To visually compare the load distribution among the gripper blocks in the clamping system, the normal clamping forces between the gripper blocks and the coiled tubing were extracted and plotted in Figure 10. Owing to the effects of the clamping-beam position and load-transfer components, such as the push plate and bracket, the actual normal clamping forces provided by gripper blocks 1–5 during operation were not uniform. When the average clamping force applied to each pair of gripper blocks was 180 kN, gripper block 1 exhibited the maximum normal clamping force of 407 kN, whereas gripper block 5 exhibited the minimum value of 189 kN. The average normal clamping force of the five gripper-block groups was 265 kN. Moreover, the normal forces of the individual gripper blocks deviated substantially from the mean value, and significant load differences were observed between adjacent gripper blocks.

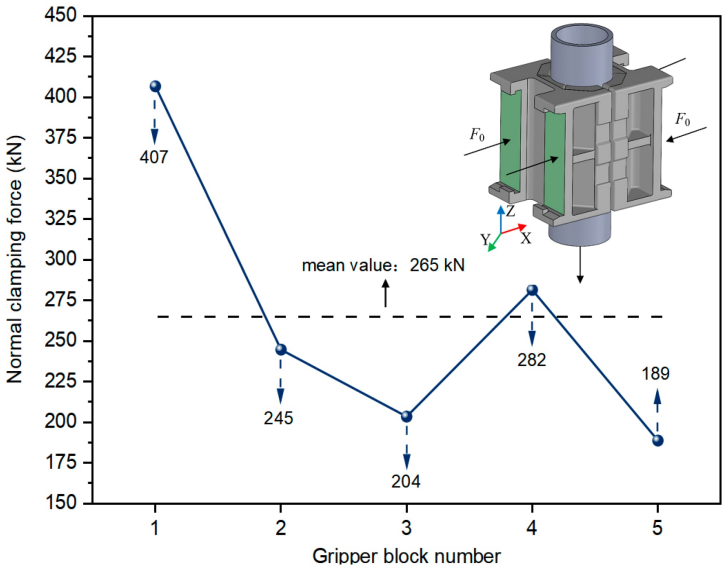


Figure 10. Normal clamping force distribution of gripper blocks at different positions in the clamping region.

3.2. Study on Straightening of Coiled Tubing Under Residual Bending

Coiled tubing is typically stored on a reel for extended periods. During operation, it undergoes six bending–straightening cycles under the action of the gooseneck, which induces plastic deformation. Consequently, a certain degree of residual curvature remains when the coiled tubing enters the injector head, as shown in Figure 11 [22]. As the stroke of the clamping hydraulic cylinders increases, the push plates on both sides of the injector-head clamping system drive the gripper blocks gradually toward the bent coiled tubing. The gripper blocks then compress the tubing to complete the straightening process.

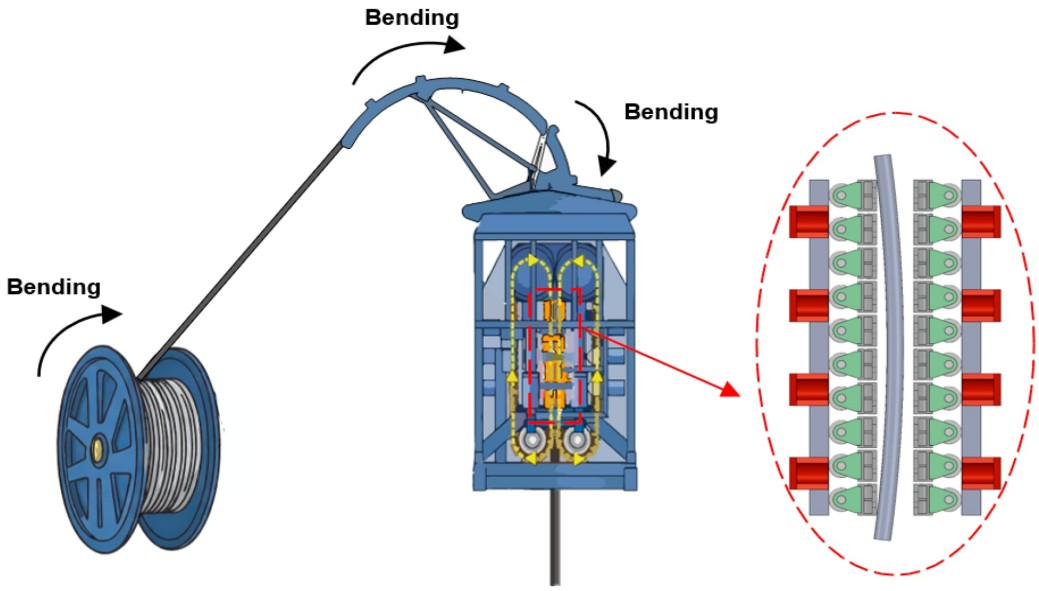


Figure 11. Schematic diagram of residual bending in coiled tubing.

Figure 12 shows the time-dependent distribution of the contact area between the gripper blocks and the coiled tubing with an initial bending radius of 6 m during the straightening process. At the initial time (t = 0 s), the coiled tubing is in a freely bent state, and no effective contact occurs between the tubing body and the gripper blocks. As the gripper blocks on both sides continuously compress the coiled tubing, contact and local compression occur at t = 0.25 s, with gripper blocks 1 and 10 acting on the inner side of the bending arc and gripper blocks 5 and 6 acting on the outer side. Subsequently, the contact region on the outer side of the bending arc expands continuously toward both ends, whereas that on the inner side expands toward the middle. Moreover, the contact area on the outer side increases at a much higher rate than that on the inner side.

During t = 0.85–0.94 s, the contact area between gripper blocks 5 and 6 and the outer side of the bending arc gradually decreases, whereas the contact area between the adjacent gripper blocks and the coiled tubing continues to increase. At t = 0.98 s, the contact area between the inner side of the bending arc and the gripper blocks begins to increase markedly, and the coiled tubing is almost completely straightened. Finally, at t = 1 s, a uniform contact band corresponding to the arrangement of the gripper blocks is formed, indicating that the coiled tubing has been fully straightened and has entered a stable contact state under further compression by the gripper blocks.

From the perspective of the mechanical mechanism, the evolution of the contact area directly reflects the deformation compatibility response of the coiled tubing. At the initial stage of deformation, only localized regions are in contact with the gripper blocks. Under the compressive action of the gripper blocks, the contact region expands along the axial direction and eventually develops into stable contact over the entire tubing section. At

t = 1 s, the coiled tubing is completely straightened, and the contact bands are uniformly spaced, showing strong agreement with the arrangement of the gripper blocks. This result indicates that the spacing between gripper blocks regulates the distribution of the contact area.

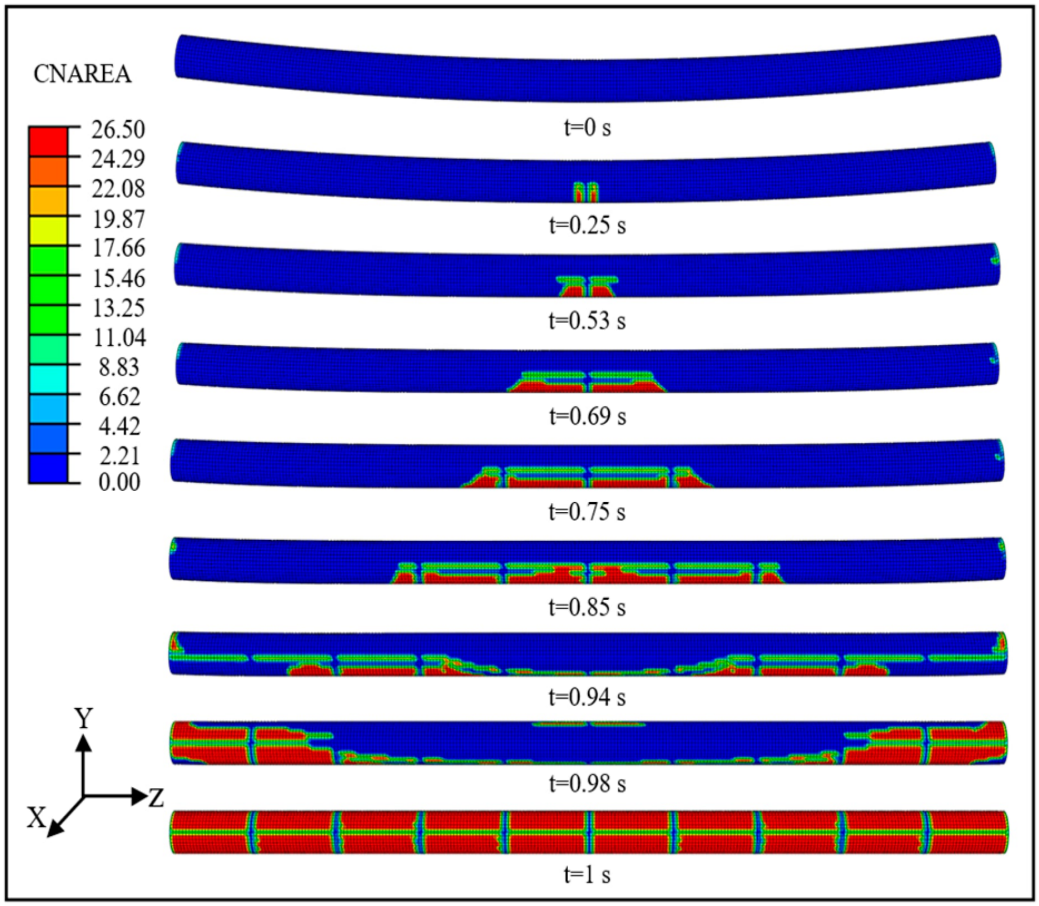


Figure 12. Contact area distribution between coiled tubing and gripper blocks during straightening.

Figure 13 shows the axial distributions of von Mises stress and strain on the inner and outer sides of the bending arc as the coiled tubing is straightened from a bent configuration. These distributions reflect the differences in mechanical response caused by the interaction between the bent tubing and multiple gripper-block groups. Moreover, significant differences in stress and strain are observed between the inner and outer sides of the bending arc. The stress distribution on the inner side is more concentrated, and the axial stress and strain levels remain higher than those on the outer side. This behavior corresponds to the larger contact area of the outer gripper blocks compared with that of the inner gripper blocks during the straightening process of the coiled tubing. As shown in Figure 9, when the coiled tubing with residual curvature is straightened, severe stress and strain fluctuations occur in the axial region of gripper block 1 on both sides of the bending arc. The stress and strain induced by gripper blocks 2–5 exhibit similarly nonuniform distributions. In addition, the average stress and strain of the coiled tubing in the bent state are much higher than those of the tubing maintained in a vertical state. Therefore, the diameter of the gooseneck bend should be increased as much as possible to reduce the residual deformation of the coiled tubing as it enters the clamping system, thereby decreasing stress concentration.

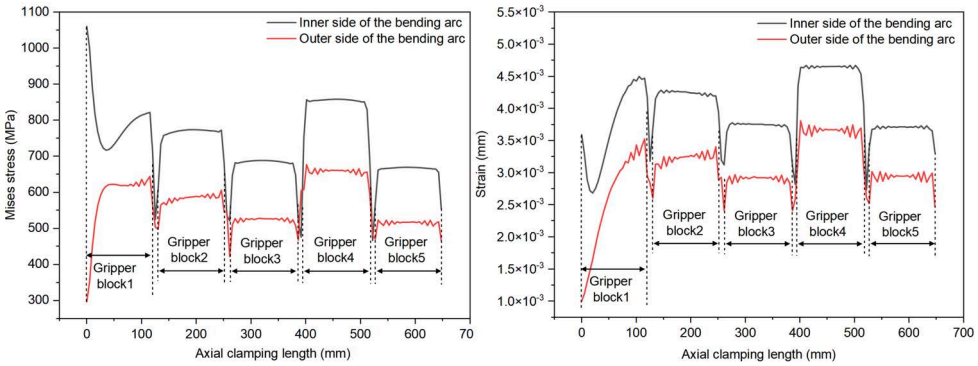


Figure 13. Stress and strain distribution in the bending arc of coiled tubing.

In actual operational cycles, residual curvature affects the load distribution among gripper blocks in two stages: during static clamping and straightening, only the gripper blocks near the ends of the bending arc initially contact and bear the load, leading to highly uneven distribution; as the clamping stroke increases and the tubing is gradually straightened, the load difference narrows, and the distribution becomes nearly identical to that of straight tubing once full straightening is achieved, with the influence of residual curvature greatly weakened. During dynamic tripping, the periodically distributed residual curvature passes through the clamping region cyclically as the coiled tubing moves axially, causing periodic load fluctuations that are most pronounced at the end gripper blocks and milder in the middle, and greater residual curvature amplifies these fluctuations to aggravate impact wear of gripper blocks and fatigue damage accumulation in the tubing.

Based on classical elastoplastic bending straightening theory, a semi-quantitative estimation indicates that reverse bending straightening leaves a self-equilibrated residual stress field in the tubing cross-section, with residual compressive stress on the outer side of the original bending arc and tensile stress on the inner side; for the studied coiled tubing with a yield strength of 758 MPa and an initial bending radius of 6 m, the peak residual stress accounts for approximately 30–50% of the yield strength, corresponding to a magnitude of 230–380 MPa. Residual stress will superimpose with clamping-induced stress, axial tensile stress and internal pressure stress to raise the overall von Mises stress level and reduce the strength safety margin to some extent, and it also accelerates fatigue damage accumulation as a mean stress under cyclic loading; nevertheless, as a global background stress after full straightening, it does not alter the load distribution ratio among individual gripper blocks, so the load distribution laws and structural optimization conclusions of this study remain unaffected.

The proposed load uniformity optimization scheme can effectively reduce the peak load fluctuation and dynamic impact induced by residual curvature, thus improving the operational stability of the clamping system in deep-well operations, and future research will introduce a cyclic plasticity constitutive model with kinematic hardening to perform refined quantitative calculation of straightening residual stress and evaluate its impact on the service life of coiled tubing combined with fatigue accumulation theory.

3.3. Effect of Gripper Block Spacing

In coiled tubing clamping operations, the gripper-block spacing is one of the key parameters governing the stress state and clamping stability of the coiled tubing. Its size directly determines the length of the clamping region, thereby affecting the overall size design of the injector head and the load-transfer characteristics along the coiled tubing. An excessively large spacing between the gripper blocks can disperse the clamping force and reduce the stability of the coiled tubing grip, whereas an excessively small spacing may

increase the risk of collision-induced damage to the injector head during operation under dynamic loads. The influence of gripper block geometric parameters on contact stress and clamping performance has been widely confirmed in previous studies on single-gripper clamping characteristics [4,8]. Therefore, identifying the effect of gripper-block spacing on system-level load uniformity is a key prerequisite for optimizing the clamping-system structure and ensuring safe coiled tubing operations. In this section, a single variable parametric analysis is conducted with gripper block spacing as the only variable. Throughout the analysis, the clamping beam spacing is fixed at 378 mm and the average clamping force is maintained at 180 kN to ensure that the observed variation in load distribution is exclusively caused by the change in gripper block spacing.

The gripper block spacing is set in the range of 2.5–15 mm, which is determined based on the conventional design range of gripper blocks for 2–3/8 in. coiled tubing injector heads. Specifically, the lower limit of 2.5 mm is set to avoid collision and interference between adjacent gripper blocks during dynamic operation, while the upper limit of 15 mm is defined to ensure sufficient clamping stability and structural rigidity of the clamping region. This range covers feasible design schemes in engineering applications.

Table 2 presents the normal force distribution of gripper blocks 1–5 under different gripper-block spacings (15–2.5 mm). The loads on the individual gripper blocks exhibit a clearly differentiated distribution pattern. Overall, the normal force on each gripper block does not fluctuate significantly and instead remains within a relatively stable range. Gripper block 1 exhibits a relatively high normal force range of 396.40–408.86 kN, whereas gripper block 5 exhibits a lower range of 186.07–195.15 kN. Consequently, the normal force difference among the gripper blocks is relatively pronounced.

Table 2. Load distribution of each gripper block under different gripper block spacings.

Normal Force (kN) / Spacing (mm)	Gripper Block 1	Gripper Block 2	Gripper Block 3	Gripper Block 4	Gripper Block 5
15	408.86	243.82	200.47	278.53	186.07
12.5	404.63	250.22	192.95	280.85	187.43
10	403.69	242.92	202.28	279.21	187.46
7.5	404.85	245.31	194.64	274.16	194.67
5	390.71	254.01	198.82	269.12	201.15
2.5	396.40	256.27	200.61	267.11	195.15

Specifically, the normal forces on gripper blocks 1 and 4 decrease slightly and fluctuate as the spacing between the gripper blocks decreases. In contrast, the normal forces on gripper blocks 2 and 5 show a gradual increasing trend with decreasing spacing. The normal force on gripper block 3 is less sensitive to spacing variations and remains within a narrow fluctuation range without any obvious upward or downward trend. Overall, under a gripper-block spacing of 15 mm, the differences in normal clamping force among the gripper blocks were relatively pronounced. As the spacing between the gripper blocks gradually decreased, the force gap between adjacent gripper blocks narrowed, and the load distribution became more uniform to some extent. Overall, the spacing between the gripper blocks exerts a differential regulatory effect on load distribution among the blocks. A smaller spacing can improve the uniformity of the load distribution to some extent, which is consistent with the variation trend of contact performance with gripper block spacing reported in similar studies [18]; however, the load level of each gripper block remains within a relatively stable range.

To more clearly evaluate the uniformity of the load distribution among the gripper blocks, the population standard deviation of the normal forces of gripper blocks 1–5 is

adopted as the quantitative load uniformity indicator. Its mathematical definition is expressed as Equation (8):

$$\sigma = \sqrt{\frac{1}{n}\sum_{i=1}^{n}\left(F_i - \overline{F}\right)^2} \tag{8}$$

where n is the total number of gripper block groups in the analysis domain ($n = 5$ in this study), F_i is the normal clamping force of the i gripper block, and $\overline{F}$ is the average normal clamping force of all gripper block groups. A smaller value of σ indicates lower dispersion of the normal force and better load distribution uniformity across the clamping system.

This metric quantitatively characterizes the dispersion of the normal forces and directly reflects the load-sharing uniformity among the gripper blocks under different gripper-block spacings. The standard deviation converts the dispersion of the load distribution into a quantitative metric, providing greater objectivity and accuracy than qualitative descriptions. In addition, it clearly characterizes the effect of gripper-block spacing on load uniformity, thereby facilitating rapid identification of the spacing range that yields the optimal load distribution.

Figure 14 shows the relationship between gripper-block spacing and the root-mean-square deviation of the normal force. As the gripper-block spacing decreases from 15 to 5 mm, the root-mean-square deviation of the normal force gradually decreases and reaches a minimum of 69.82 kN at 5 mm. At this spacing, the load distribution among the gripper blocks exhibits the lowest dispersion and the highest uniformity. However, when the gripper-block spacing is further reduced to 2.5 mm, the root-mean-square deviation increases markedly. Consequently, the differences in normal force among the gripper blocks increase again, leading to greater unevenness in the load distribution.

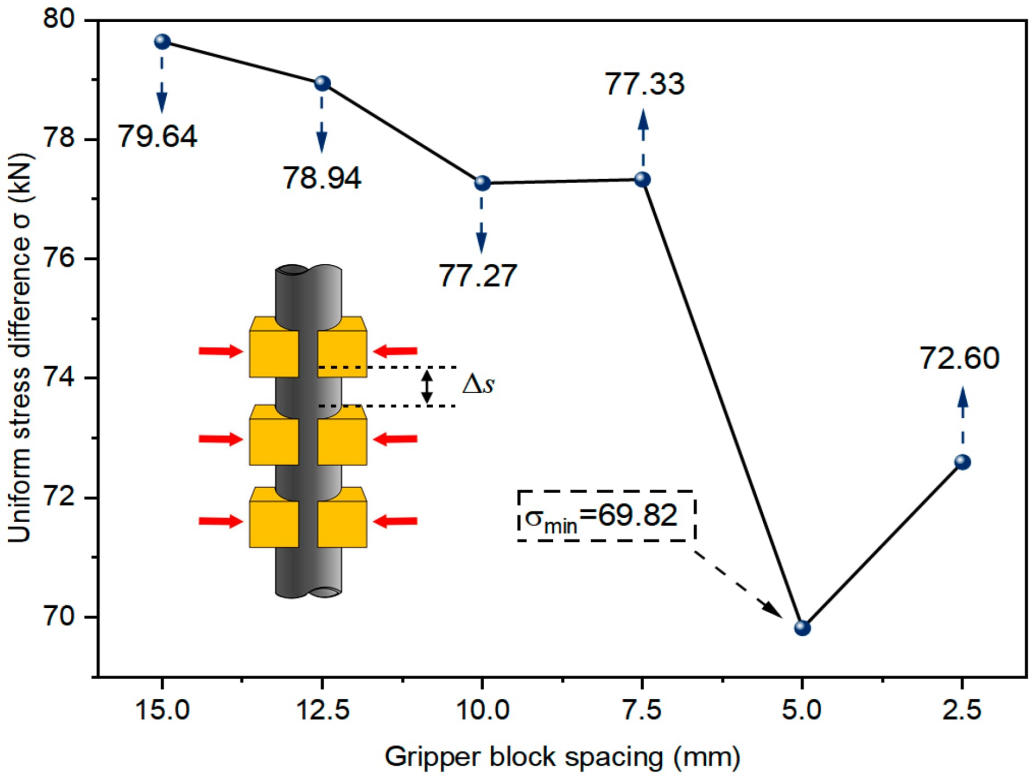


Figure 14. Effect of gripper block spacing on load distribution uniformity.

Figure 15 shows the variations in the maximum von Mises stress and maximum contact pressure of the coiled tubing as a function of gripper-block spacing. As the gripper-block spacing gradually decreases from 15 mm to 2.5 mm, the maximum von Mises stress of

the coiled tubing shows a slight downward trend and remains within a narrow range of 130–140 MPa, with no significant fluctuations. The maximum contact pressure on the coiled tubing increases gradually as the gripper-block spacing decreases, rising from 41.4 MPa at a spacing of 15 mm to 44.3 MPa at a spacing of 2.5 mm. When the gripper-block spacing is large, the stress change between the contact zones where each gripper-block group compresses the coiled tubing and the gap zones between adjacent gripper blocks and the coiled tubing is pronounced. Under these conditions, the stress distribution is relatively concentrated, whereas the contact pressure is more dispersed. As the spacing decreases, the compression zones of the gripper blocks become progressively denser, the local stress concentration in the coiled tubing is slightly alleviated, and the pressure in the contact zones increases gradually.

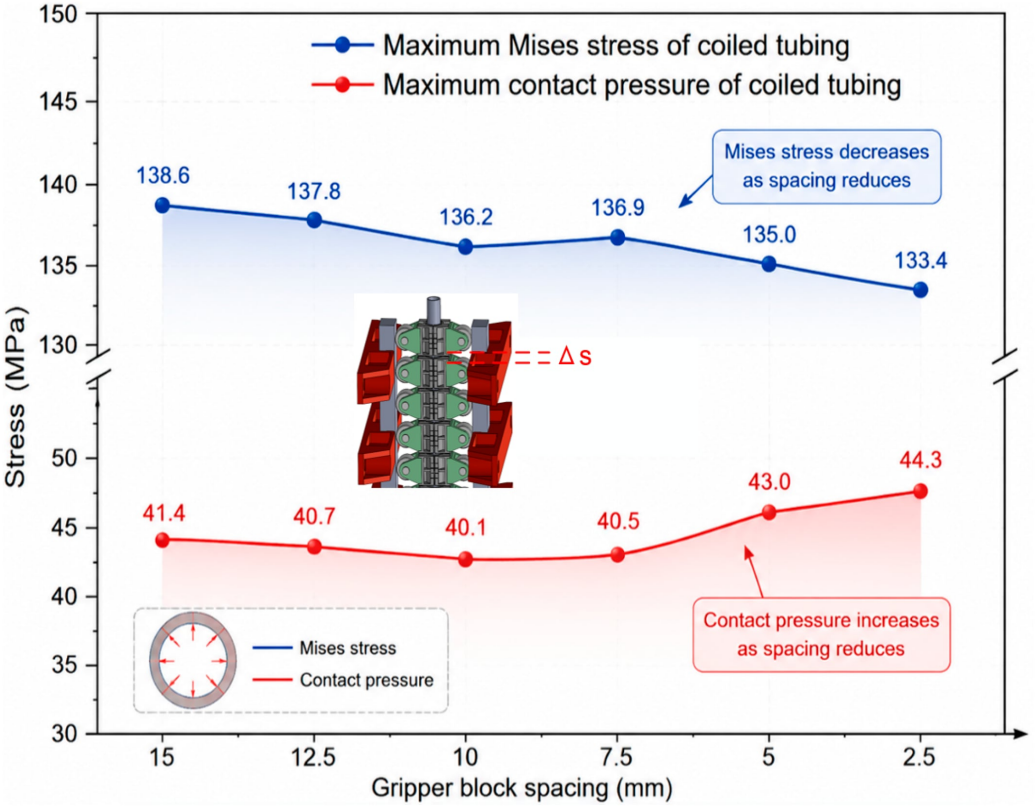


Figure 15. Effect of gripper block spacing on the von Mises stress and contact pressure of coiled tubing.

It should be noted that the gripper block normal load, surface contact pressure, and von Mises equivalent stress of the coiled tubing present distinct distribution characteristics and variation trends, which are essentially determined by their different physical connotations and mechanical action levels.

From the perspective of the action scale, the normal clamping force of each gripper block is a macroscopic global load obtained by integrating contact pressure over the entire contact interface. Its axial distribution pattern is dominated by the bending deflection of the push plate in the force transmission chain, showing the overall characteristic of "high values at both ends and low values in the middle". The overall load level directly determines the magnitude order of contact pressure and tubing stress.

In contrast, contact pressure is a local surface mechanical quantity acting on the outer wall of the tubing, and its magnitude and distribution are jointly affected by the total load of the gripper block, the contact fit state of the interface and the local deformation of the

material. Even on the contact surface of a single gripper block, the contact pressure presents a non-uniform distribution of "high at the edge and low in the center" due to the edge effect of elastic contact.

The von Mises equivalent stress is a comprehensive equivalent quantity reflecting the three-dimensional stress state inside the tubing wall. It is synthesized from radial stress, hoop stress and axial stress, so its magnitude and peak position are not completely consistent with the contact pressure. Under local clamping load, the maximum contact pressure appears on the outer wall contact surface, while the maximum von Mises stress occurs on the inner wall at the gap between adjacent gripper blocks, which is caused by the superposition of hoop tensile stress and axial compressive stress along the wall thickness direction.

In general, the three quantities are interrelated: the gripper block load determines the overall load input, contact pressure is the direct interface manifestation of the load, and von Mises stress is the final mechanical response inside the tubing. The load uniformity optimization of the clamping system essentially reduces the overall dispersion of tubing stress by improving the load uniformity among gripper blocks, so as to avoid local overload damage.

3.4. Effect of Clamping Beam Spacing

In the injector head clamping system, the clamping beam is a critical structural component that bears and transmits the clamping force. Its spacing directly determines the stress state of multiple gripper blocks. Changes in the spacing of the clamping beams alter the distribution of clamping force among the gripper blocks by changing the bending deflection of the push plate, and this load transmission mechanism is universal in multi-point clamping structures [11]. Therefore, investigating the load distribution among the gripper blocks and the stress state of the coiled tubing under different clamping-beam spacings provides an important basis for optimizing the clamping system structure and ensuring safe and efficient coiled tubing operations. For the single-variable analysis of clamping beam spacing in this section, the gripper block spacing is fixed at 2.5 mm, and the average clamping force is kept constant at 180 kN. This control variable setting eliminates interference from other structural parameters and ensures the independence of the analysis results.

The clamping beam spacing is selected from 252 mm to 378 mm, which is constrained by the total length of the push plate (1260 mm) and the layout of 4 clamping beams. This range covers all feasible arrangement schemes from relatively dispersed layout to compact layout, and fully considers the structural installation space of hydraulic cylinders and the bending stiffness requirement of the push plate. The optimal equal-spacing scheme (315 mm) is also included in this range.

Table 3 presents the distribution of normal forces on gripper blocks 1–5 as the clamping-beam spacing gradually decreases from 378 mm to 252 mm, that is, as the push plate moves progressively from both ends toward the center. It can be seen that the loads on the gripper blocks exhibit distinctly different trends as the clamping beam spacing decreases. The normal force on gripper block 1 decreases continuously as the clamping beam spacing decreases, falling from 396.40 kN at the maximum spacing of 378 mm to 96.98 kN at a spacing of 252 mm. Among all gripper blocks, it shows the most pronounced force reduction. The normal force on gripper block 2 exhibits slight fluctuations overall. As the spacing decreases, it first increases from 256.27 kN to 297.70 kN and then decreases to 250.97 kN. In contrast, the normal forces on gripper blocks 3, 4, and 5 increase continuously as the spacing decreases. Specifically, the force on gripper block 3 rises from 200.61 kN to 311.81 kN, that on gripper block 4 increases from 267.11 kN to 332.05 kN, and that on gripper block

5 increases from 195.15 kN to 335.11 kN. Moreover, the increase becomes progressively greater as the spacing decreases.

Table 3. Load distribution of each gripper block under different clamping beam spacings.

Normal Force (kN) / Spacing (mm)	Gripper Block 1	Gripper Block 2	Gripper Block 3	Gripper Block 4	Gripper Block 5
378	396.40	256.27	200.61	267.11	195.15
357	355.32	267.04	209.20	288.32	208.59
336	302.66	283.89	218.92	294.14	230.97
315	284.68	297.70	236.17	285.70	214.48
294	191.62	295.54	259.09	306.55	278.46
273	143.94	280.89	283.34	316.48	305.33
252	96.98	250.97	311.81	332.05	335.11

Figure 16 shows the variation in the root-mean-square deviation of the normal forces on gripper blocks 1–5 as a function of clamping beam spacing. As the clamping beam spacing decreases from 378 mm to 315 mm, the root-mean-square deviation decreases continuously and reaches a minimum of 32.43 kN at 315 mm. Compared with the initial value of 72.60 kN at the spacing of 378 mm, the root-mean-square deviation is reduced by approximately 55.3%, indicating a substantial improvement in load distribution uniformity. At this point, the clamping beam spacing is equal to the pusher plate length divided by the number of clamping beams. However, when the clamping beam spacing is further reduced from 315 mm to 252 mm, the root-mean-square deviation of the normal force rapidly increases to 89.48 kN. This indicates a pronounced increase in the dispersion of normal force among the gripper blocks, leading to a marked deterioration in load-distribution uniformity. This is because, as the clamping-beam spacing decreases, the layout of the clamping beams becomes more compact. Consequently, the load originally concentrated on the end gripper blocks (e.g., gripper block 1) is gradually transferred to the middle gripper blocks in the system (e.g., gripper blocks 3–5). During this process, the loads carried by the end and middle gripper blocks undergo a dynamic redistribution, with one increasing as the other decreases.

This trend clearly demonstrates the regulating effect of clamping-beam spacing on the load distribution of the gripper blocks. As shown in Figure 16, the optimal clamping-beam spacing is 315 mm, which equals the pusher-plate length divided by the number of clamping beams. At this spacing, the load distribution is the most uniform. However, when the spacing deviates from this optimal value, either by increasing or decreasing, the load dispersion among the gripper blocks increases, resulting in poorer distribution uniformity.

Figure 17 shows the variations in the maximum von Mises stress and maximum contact pressure of the coiled tubing as a function of clamping-beam spacing. As the clamping-beam spacing decreases from 378 mm to 252 mm, the maximum von Mises stress of the coiled tubing first decreases sharply and then rises slightly. Specifically, it drops from 136.40 MPa at 378 mm to 101.30 MPa at 336 mm and subsequently fluctuates slightly within the range of 100–110 MPa. In contrast, the maximum contact pressure on the coiled tubing shows a trend of a gradual decrease followed by stabilization. It decreases from 41.60 MPa at a clamping-beam spacing of 378 mm to 34 MPa at 315 mm and then remains at approximately 33 MPa. This is because, when the clamping beam spacing is relatively large, the load is concentrated on the end gripper blocks; consequently, the maximum von Mises stress in the coiled tubing remains at a relatively high level, and the peak contact pressure is also high. As the clamping beam spacing decreases, the beam layout becomes more compact, the load distribution among the gripper-block groups becomes more uniform, and both the maximum von Mises stress and the contact pressure in the coiled tubing decrease.

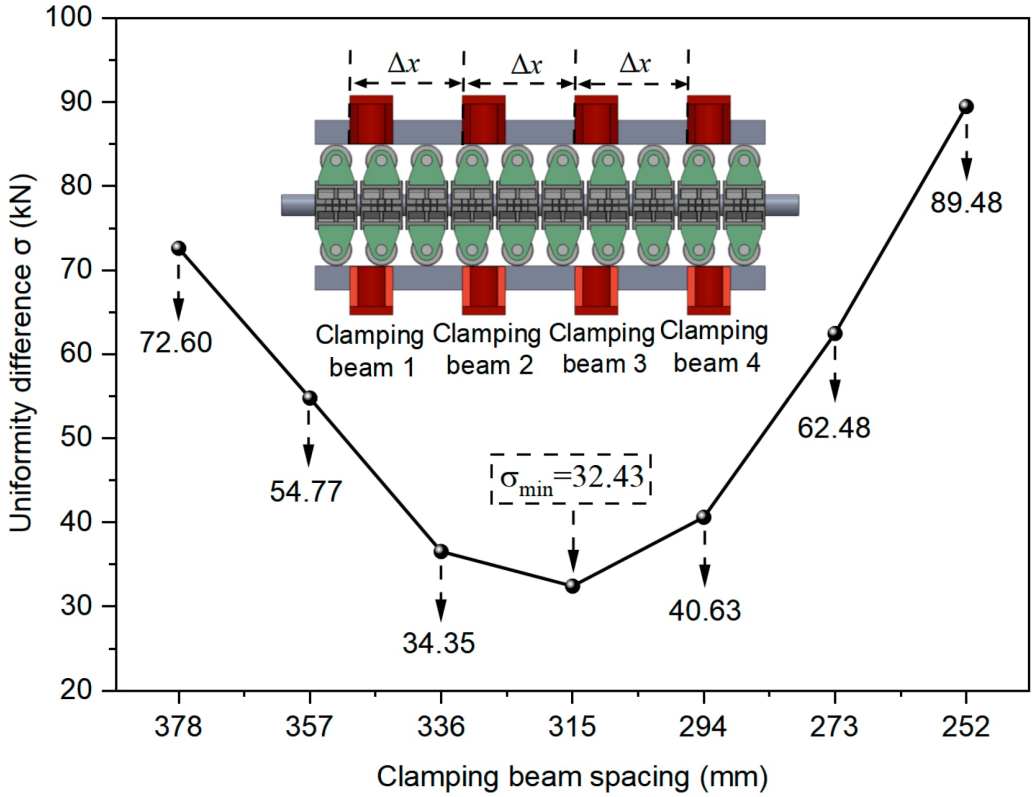


Figure 16. Effect of clamping beam spacing on load distribution uniformity.

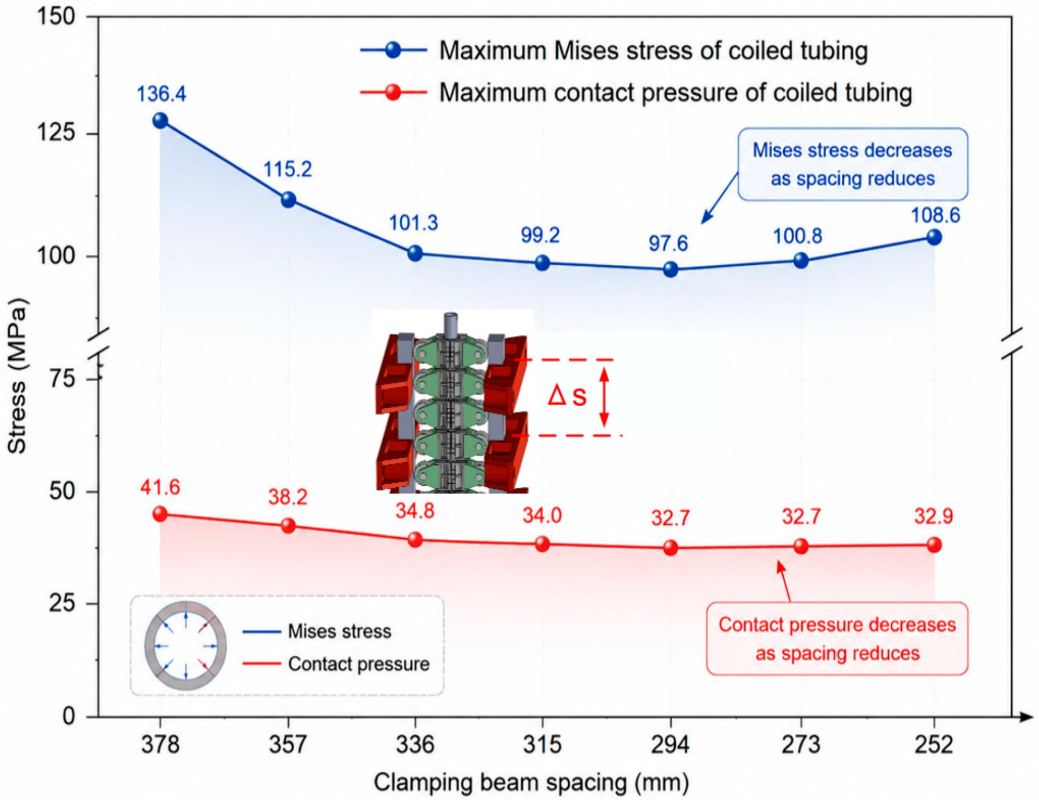


Figure 17. Effect of clamping beam spacing on the von Mises stress and contact pressure of coiled tubing.

It should be noted that the optimal clamping beam spacing of 315 mm obtained in this study is a quantitative result derived from the specific structural model with a push plate length of 1260 mm, 4 clamping beams, 10 pairs of effective gripper blocks, and 2–3/8 in. coiled tubing, which can be directly applied to the clamping system design of injector heads with the same specifications.

From the perspective of mechanical essence, the design principle that the optimal clamping beam spacing equals the ratio of push plate length to the number of clamping beams (i.e., clamping beams are arranged at equal intervals along the push plate) is universally applicable. This conclusion conforms to the bending deformation law of multi-supported beams in structural mechanics, and has also been verified in the design optimization of similar coiled tubing injector head clamping mechanisms [5]. This conclusion originates from the bending deformation law of beams subjected to multiple concentrated loads. When clamping beams act on the push plate at equal intervals, the bending deflection distribution of the push plate along the axial direction is the most uniform, and the difference in reaction forces borne by each roller–carrier–gripper block assembly is minimized, resulting in the optimal uniformity of normal loads transmitted to each gripper block. This mechanical law is not affected by geometric parameters such as push plate length, number of clamping beams, and tubing specifications, and is applicable to the design of coiled tubing injector head clamping systems with different tonnages and specifications.

For injector heads with other configurations, the equal-spacing arrangement principle can be followed to determine the initial design scheme, and local fine-tuning can be carried out through finite element simulation combined with specific structural parameters to obtain the optimal clamping beam spacing for load uniformity under the corresponding structure.

3.5. Effect of Clamping Force

In the clamping system, the clamping force directly determines the normal contact force between the gripper blocks and the coiled tubing, as well as the efficiency of load transmission. On the one hand, analyzing the load distribution under different clamping forces helps clarify the effect of clamping force magnitude on the normal-force distribution among the gripper blocks. It also verifies whether, under the parameter combination of a 5 mm gripper-block spacing and a 315 mm clamping-beam spacing, different clamping forces can still maintain favorable load-distribution characteristics. On the other hand, by analyzing the relationship between the total clamping normal force under different clamping forces and downhole depth, a basis can be directly provided for selecting the appropriate clamping force for operations at different depths.

The average clamping force is set in the range of 100–300 kN, which corresponds to the actual operating range of the target injector head from conventional working conditions to rated load conditions. The lower limit covers the clamping demand for shallow well operations, while the upper limit matches the maximum output capacity of the hydraulic system. This range covers common working scenarios in field coiled tubing operations.

Based on the above analysis, the load distribution in the clamping system is most uniform when the gripper-block spacing is 5 mm, and the clamping-beam spacing is 315 mm. Table 4 presents the distribution of normal forces on gripper blocks 1–5 at this spacing as the average clamping force increases from 100 kN to 300 kN. As the average clamping force increases, the normal forces on all gripper blocks increase linearly. This indicates that an increase in clamping force correspondingly enhances the load carried by each gripper block, and the load transfer exhibits good linear stability under this parameter setting. At different clamping-force levels, the relative difference in normal force between adjacent gripper blocks increases as the average clamping force increases. This suggests that increasing the

average clamping force exacerbates the inherent differences in load distribution among the gripper blocks.

Table 4. Load distribution of each gripper block under different clamping forces.

Average Clamping Force (kN) \ Normal Force (kN)	Gripper Block 1	Gripper Block 2	Gripper Block 3	Gripper Block 4	Gripper Block 5
100	160.13	169.75	144.45	155.86	122.10
140	223.86	235.68	193.45	219.84	169.32
180	284.68	297.70	236.17	285.70	214.48
220	345.57	358.08	287.26	347.50	250.89
260	411.17	421.39	337.40	413.25	295.05
300	472.52	481.03	385.89	475.07	334.14

Figure 18 shows the variation in the average clamping force and the root-mean-square deviation of the normal forces on the gripper blocks for the clamping system at a gripper-block spacing of 5 mm and a clamping-beam spacing of 315 mm. As shown in the figure, as the average clamping force increases from 100 kN to 300 kN, the root-mean-square deviation exhibits an approximately linear and continuous upward trend. Specifically, it increases from 16.34 kN at 100 kN to 59.29 kN at 300 kN, indicating that load-distribution uniformity deteriorates progressively with increasing clamping force. This trend reflects the dynamic effect of clamping force on load-distribution uniformity. The underlying reason is the inherent difference in load sharing among the gripper blocks. When the clamping force is small, this absolute difference is also small, resulting in low load dispersion. However, as the clamping force increases, the normal force on each gripper block increases proportionally, and the inherent difference is amplified linearly.

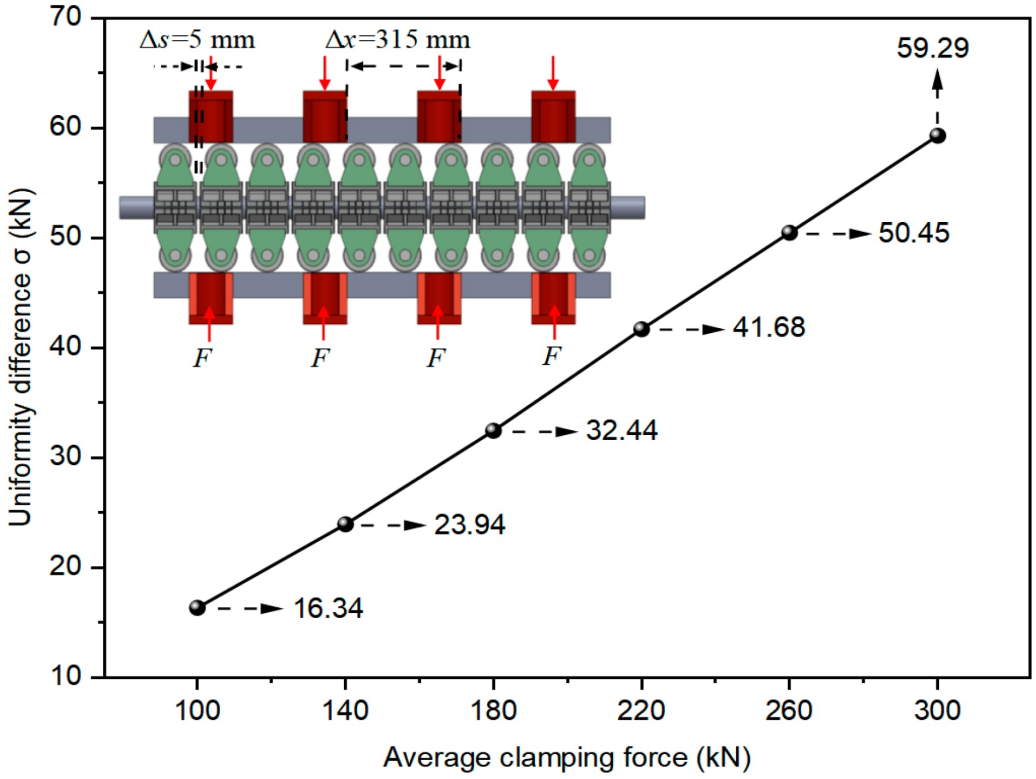


Figure 18. Effect of average clamping force on load distribution uniformity.

Under a gripper-block spacing of 5 mm and a clamping-beam spacing of 315 mm, the variations in the maximum von Mises stress and maximum contact pressure of the

coiled tubing with average clamping force are shown in Figure 19. As the average clamping force increases, both the maximum von Mises stress and the maximum contact pressure in the coiled tubing increase linearly. This is because, under the compression of multiple gripper-block groups, the overall load borne by the coiled tubing increases with increasing clamping force, leading to a linear accumulation of stress. Although the load distribution is relatively uniform under the current parameter combination, a further increase in clamping force still causes the overall stress in the coiled tubing to rise rapidly, highlighting the significant effect of clamping force on the structural stress of the coiled tubing.

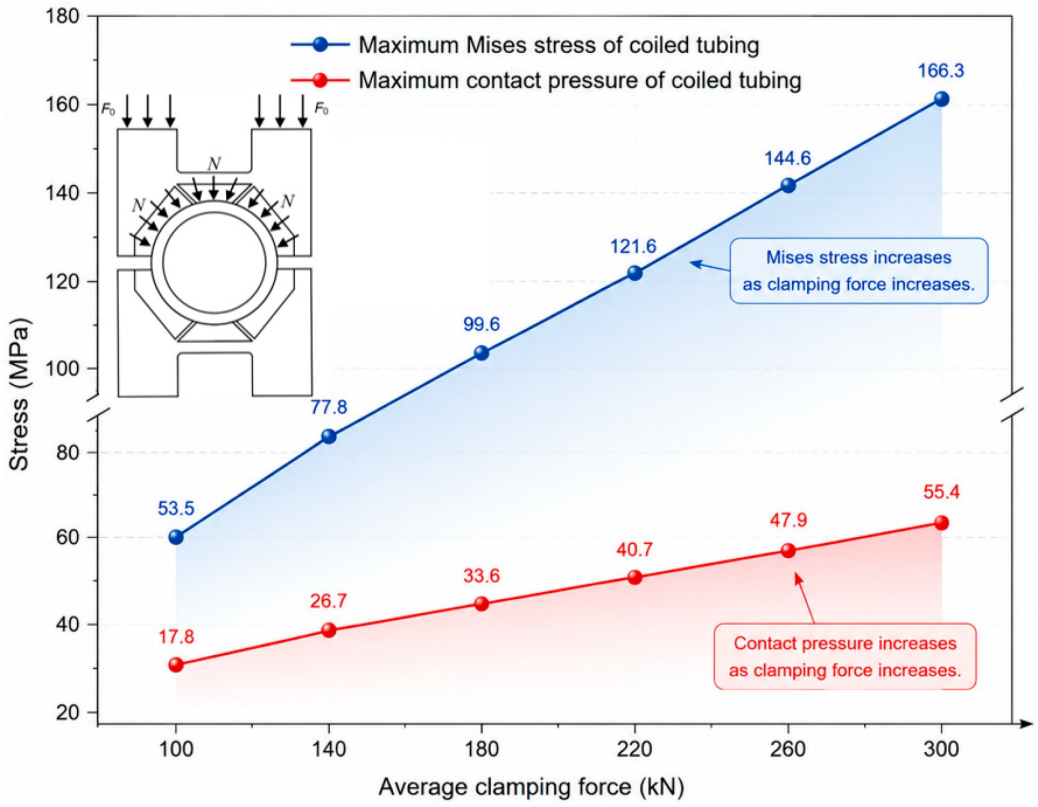


Figure 19. Effect of average clamping force on the von Mises stress and contact pressure of coiled tubing.

Based on the load distribution laws obtained in this study, a specific criterion for clamping force selection with well depth and tubing string weight as core inputs has been supplemented. The core design principle is that the maximum static friction force provided by all gripper blocks of the clamping system must exceed the maximum axial load of the coiled tubing at the corresponding well depth, with a reasonable safety margin reserved. The specific selection procedure is as follows: first, according to the target operating well depth, coiled tubing specifications, drilling fluid density and wellbore pressure, the maximum axial load under the tubing pull-out condition, which covers the tubing string self-weight, wellbore upward force and axial friction resistance, is calculated via the axial force calculation model established in Section 2.2. Subsequently, based on the friction equilibrium relationship and combined with the friction coefficient between the gripper blocks and the tubing as well as the friction amplification coefficient of the transmission mechanism, the required total normal clamping force is derived inversely. Finally, considering the load uniformity level of the clamping system, the output thrust of each set of clamping cylinders is determined through load allocation. The load uniformity optimization scheme proposed in this work can avoid local overload of individual gripper blocks under the same total

clamping force input, and equivalently improve the overall load-bearing capacity of the clamping system. In deep-well high-load operation scenarios, the optimized structure can satisfy operational safety requirements with lower cylinder thrust, or achieve a higher safety margin under the same thrust configuration.

It should be noted that all the parametric analyses above are carried out with the single-variable control method, to clarify the independent regulatory effect of each parameter on the load distribution characteristics of the clamping system. In actual engineering scenarios, there exist certain interaction effects among gripper block spacing, clamping beam spacing and clamping force. Specifically, an increase in clamping force will aggravate the bending deflection of the push plate, which further amplifies the influence of clamping beam spacing on load uniformity; when the gripper block spacing is smaller, the overall load distribution is more sensitive to variations in clamping beam spacing.

Limited by the research scope and analytical framework of this work, a comprehensive quantitative investigation of multi-parameter coupling interactions is not performed in the current manuscript. In follow-up studies, orthogonal experimental design and response surface methodology will be adopted to systematically explore the coupling interaction mechanism among multiple parameters, and further obtain the global optimal parameter matching scheme for the clamping system.

The above-derived optimal structural parameters for load uniformity are closely oriented toward the actual demands of deep-well coiled tubing operations. In deep-well scenarios, the coiled tubing bears large axial tensile loads, and the injector head must provide sufficiently high total clamping normal force to avoid tubing slippage [23]. As demonstrated in Figure 18, higher clamping force will amplify the load dispersion among individual gripper blocks, which further aggravates local overloading and stress concentration on the coiled tubing. The proposed optimization scheme (5 mm gripper-block spacing and equal-interval clamping-beam layout) suppresses this load-dispersion amplification effect under large clamping-force levels. Under the same total applied clamping force, it reduces the peak normal force borne by partial gripper blocks and lowers the peak von Mises stress of the tubing.

For practical deep-well applications: when designing an injector head for deep-well service, the recommended parameter combination can be adopted as the baseline design. For wells with different tubing specifications, push-plate dimensions and clamping-beam quantities, the equal-spacing arrangement principle for clamping beams can still be followed, while fine-tuning via finite-element simulation is required to match site-specific operating conditions. The clamping-force selection procedure described above can be combined with real-time down-hole axial load calculated from well depth, tubing weight and wellbore pressure, to realize the matching between structural optimization output and field deep-well operating requirements.

4. Conclusions

This study focuses on the issues of injector-head gripping performance and load-distribution uniformity in coiled tubing operations from three aspects: theoretical mechanical analysis, numerical simulation and parameter optimization, and regulation of load-distribution uniformity in the clamping system. The gripping mechanism was clarified, and the load-distribution characteristics of the gripper blocks, as well as the effects of key parameters on load-distribution uniformity, were systematically investigated. The key findings of this research are summarized as follows:

(1) A transmission model from clamping force to normal clamping force was established, revealing the key factors governing the load distribution in the clamping system. It also clarified the regulatory mechanism by which structural parameters, including gripper-

block spacing and clamping-beam spacing, affect load sharing, thereby providing a theoretical basis for subsequent analysis of load-distribution patterns and parameter optimization.

(2) By analyzing the stress–strain distribution of the coiled tubing under bending, it was found that a significant mechanical asymmetry exists between the inner and outer sides of the bent arc. Specifically, due to the compressive effect, the stress and strain levels on the inner side are higher than those on the outer side and are also much higher than those when the coiled tubing remains in a vertical state. Therefore, the diameter of the guide-arch curvature should be increased as much as possible to reduce the residual deformation of the coiled tubing before it enters the clamping system.

(3) Under the coordinated action of the clamping system, the loads transmitted by each gripper block are unevenly distributed; within the studied clamping force range of 100–300 kN and under the optimal combination of gripper block spacing and clamping beam spacing, the standard deviation of the normal forces increases approximately linearly with the clamping force. Adjusting the gripper block spacing and clamping beam spacing can significantly improve the load distribution uniformity of the clamping system and reduce the risk of local stress concentration in the coiled tubing. Among them, the design principle of equidistant arrangement of clamping beams is universal and applicable to injector head structures of different specifications. For the research model in this work, the optimal parameters are obtained as follows: the clamping beam spacing is equal to the ratio of the push plate length to the number of clamping beams, and the gripper block spacing is 5 mm, under which the load distribution of the clamping system is the most uniform.

Author Contributions: G.Y.; Software, Data Curation, Writing—original draft, Funding acquisition; H.J.; Writing—original draft, Investigation, Methodology; F.L.; Funding acquisition, Formal analysis; Z.G.; Investigation, Validation; W.Y.; Validation. J.L.: Methodology, H.W.; Writing—review and editing, C.C.; Formal analysis. All authors have read and agreed to the published version of the manuscript.

Funding: This research was funded by the National Natural Science Foundation Project, grant number 42472383.

Data Availability Statement: The data presented in this study are available on request from the corresponding author.

Conflicts of Interest: Authors Gao Yang, Fei Liu, Zhiliang Gai, Wencai Yuan and Jiawei Liu were employed by the Jianghan Machinery Research Institute Co., Ltd., China National Petroleum Corporation (CNPC). The remaining authors declare that the research was conducted in the absence of any commercial or financial relationships that could be construed as potential conflicts of interest.

References

1. He, D.; Jia, C.; Zhao, W.; Xu, F.; Luo, X.; Liu, W.; Tang, Y.; Gao, S.; Zheng, X.; Li, D.; et al. Research progress and key issues of ultra-deep oil and gas exploration in China. *Pet. Explor. Dev.* **2023**, *50*, 1333–1344. [CrossRef]
2. Livescu, S.; Craig, S.; Watkins, T. Challenging the industry's understanding of the mechanical friction reduction for coiled tubing operations. In Proceedings of the SPE Annual Technical Conference and Exhibition, Amsterdam, The Netherlands, 27–29 October 2014. [CrossRef]
3. Perry, K. Microhole coiled tubing drilling: A low cost reservoir access technology. *J. Energy Resour. Technol.* **2009**, *131*, 013104. [CrossRef]
4. Liu, S.H.; Zhou, H.; Ma, W.G.; Xin, Y.A.; Yang, Z.C.; Du, K. Development and application of a coiled tubing fatigue life prediction software. *China Pet. Mach.* **2020**, *48*, 135–140. [CrossRef]
5. Urdaneta, C.; Shah, A.B.; Wu, X.; Fu, X.; Chen, J. Coiled-tubing drilling dynamics forecasting. In *Deep Learning Applications for Drilling Performance: Forecasting, Diagnostics, Telemetry, and Predictive Maintenance*; Springer: Cham, Switzerland, 2026; pp. 45–56. [CrossRef]
6. Huang, Y.; Liu, B.; Yang, G.; Liu, H.; Zhang, Y. Fatigue damage model of CT110 coiled tubes: From material characterization to generalized prediction. *J. Braz. Soc. Mech. Sci. Eng.* **2026**, *48*, 26. [CrossRef]

7. Liu, S.; Yang, Y.; Wu, W.; Huang, R.; Lei, L.; Zhong, L. Study on friction and wear failure mechanism of coiled tubing and casing at high temperature. *Mater. Today Commun.* **2025**, *48*, 113454. [CrossRef]
8. Sun, S.; Liu, J.; Sang, R.; Zhao, K. Experimental study of flow friction behavior in coiled tubing. *Energy Rep.* **2022**, *8*, 187–196. [CrossRef]
9. Wang, H.; Huang, H.; Bi, W.; Ji, G.; Zhou, B.; Zhuo, L. Deep and ultra-deep oil and gas well drilling technologies: Progress and prospect. *Nat. Gas Ind. B* **2022**, *9*, 141–157. [CrossRef]
10. Tong, S.; Gao, D.; Yue, Y. Dynamic response of coiled tubing perforation under unstable fluid injection. *Arab. J. Sci. Eng.* **2019**, *44*, 10467–10480. [CrossRef]
11. Shah, S.N.; Jain, S. Coiled tubing erosion during hydraulic fracturing slurry flow. *Wear* **2008**, *264*, 279–290. [CrossRef]
12. Yin, Z.; Zhang, F.; Yuan, W. Research and design of injection head clamping device. *Int. J. Precis. Eng. Manuf.* **2025**, *26*, 1715–1732. [CrossRef]
13. Carpenter, C. Study explores mechanisms of surface damage on coiled tubing. *J. Pet. Technol.* **2019**, *71*, 56–57. [CrossRef]
14. Goode, J. Coiled Tubing Injector. UK Patent GB2324948A, 9 December 1998.
15. Hu, Z.Q.; Liu, S.J.; Yuan, W.C.; Yang, G.; Liu, F.; Duan, W.Y. Research on gripping performance of CT injector head gripper block and structure optimization. *China Pet. Mach.* **2019**, *47*, 69–74. [CrossRef]
16. Zhang, D.Y.; Zhang, C.; Hu, Z.W. Mechanical analysis and structural optimization of injector head gripper blocks for coiled tubing. *Oil Field Equip.* **2017**, *46*, 1–6. [CrossRef]
17. Yang, G.; Liu, F.; Tang, C.J. Study on the clamping performance of gripper blocks in a coiled tubing injector head. *China Pet. Mach.* **2012**, *40*, 10–14. [CrossRef]
18. Zheng, W. Mechanical analysis and structural optimization of the clamping system of a coiled tubing injector head. *Shandong Chem. Ind.* **2019**, *48*, 3.
19. Zhang, J.Z. Research on Improving the Service Life of Chain Bearings in Coiled Tubing Injector Heads. Master's Thesis, China University of Petroleum (Beijing), Beijing, China, 2023. [CrossRef]
20. Wang, A.Y.; Liang, Z.; Wu, D.F. Calculation and analysis of friction resistance in coiled tubing downhole operations. *China Pet. Mach.* **2010**, *38*, 25–27, 31, 94. [CrossRef]
21. Zhao, Z.M. *Handbook of Coiled Tubing Engineering Technology*; Petroleum Industry Press: Beijing, China, 2011.
22. Tipton, S.M.; Smalley, E.; VanArnam, D. Influence of a straightener on coiled tubing fatigue. In Proceedings of the SPE/ICoTA Coiled Tubing & Well Intervention Conference and Exhibition, The Woodlands, TX, USA, 27–28 March 2012. [CrossRef]
23. Ilyushin, Y.; Martirosyan, A.V.; Asadulagi, M.-A.; Kukharova, T. Modeling and optimization of an automatic temperature control system for the catalytic cracking process. *Modelling* **2026**, *7*, 68. [CrossRef]

Disclaimer/Publisher's Note: The statements, opinions and data contained in all publications are solely those of the individual author(s) and contributor(s) and not of MDPI and/or the editor(s). MDPI and/or the editor(s) disclaim responsibility for any injury to people or property resulting from any ideas, methods, instructions or products referred to in the content.